PHYSICAL REVIEW A **92**, 013415 (2015)

Isolating resonant excitation from above-threshold ionization

Yun Shao,[1] Min Li,[1,2] Ming-Ming Liu,[1] Xufei Sun,[1] Xiguo Xie,[1] Peng Wang,[1] Yongkai Deng,[1]
Chengyin Wu,[1,3] Qihuang Gong,[1,3] and Yunquan Liu[1,3,*]
[1]*Department of Physics and State Key Laboratory for Mesoscopic Physics, Peking University, Beijing 100871, China*
[2]*Wuhan National Laboratory for Optoelectronics and School of Physics, Huazhong University of Science and Technology, Wuhan 430074, China*
[3]*Collaborative Innovation Center of Quantum Matter, Beijing 100871, China*

(Received 13 May 2015; published 17 July 2015)

We measure photoelectron energy distributions from single ionization of xenon atoms by a linearly polarized laser pulse (800 nm, 25 fs) with successively varying the laser intensity within the region of $1.4 - 7.0 \times 10^{13}$ W/cm^2. By measuring the photoelectron energy shifted with the ponderomotive potential, we have calibrated the laser peak intensity precisely with an uncertainty less than 5%. Employing the quantum trajectory Monte Carlo theory, we simulate the photoelectron energy spectra with respect to the laser intensity. By comparison between the measurement and the simulation, we are able to identify resonant structures from photoelectron energy spectra in the low-energy region, which do not shift with the laser intensity. Inspecting the momentum distribution along the laser propagation axis, we have further shown that the quantum interference effect has a significant effect on the width of the momentum distribution perpendicular to the laser polarization direction beside the Coulomb focusing effect.

DOI: 10.1103/PhysRevA.92.013415 PACS number(s): 32.80.Fb, 32.80.Rm

I. INTRODUCTION

Above-threshold ionization (ATI) has attracted considerable attention since its first observation more than 30 years ago [1], in which an atom exposing in a strong laser field can absorb more photons than the minimum necessary numbers to reach the ionization limit. Thus, ATI manifests itself as many peaks separated by one photon in the photoelectron energy spectrum. Owing to the ponderomotive shift of the Rydberg states close to the ionization limit, these highly populated excited states will shift upward by approximately U_p [2] (U_p is the ponderomotive potential given by $U_p = E_0^2/4\omega^2$, where E_0 is the laser field amplitude and ω is its frequency; atomic units are used throughout unless otherwise specified). At a specific intensity, they may come into resonance by absorbing a certain number of photons from the ground state. This resonant ionization has been observed in the electron spectra when the ac Stark shift resonantly excited states absorb one more photon into the continuum [3]. The resonant structures are usually embedded in the photoelectron energy spectra, which are hard to identify. Recently, it was theoretically shown that the contributions of the resonant excited states can be identified by Fourier transform of the two-dimensional momentum spectra [4]. As is well known, the ATI peaks will shift with respect to the laser intensity, and the nonresonant ATI peaks will shift towards low energies as the laser intensity increases. The resonantly enhanced ionization via the intermediate Rydberg states in the multiphoton regime will be independent of the laser intensity [5,6]. Actually, the laser intensity stands as a crucial parameter for the accurate comparison between quantitative simulations with experimental measurement. In recent years, several methods have been developed to calibrate the laser intensity. A simplistic but instructive estimation of the laser intensity is fitting the experimental data of the electron kinetic energy spectra with the Ammosov-Delone-Krainov (ADK) tunneling rate for single ionization [7]. Alnaser *et al.* [8] put forward another method to calibrate the laser peak intensity by comparing the photon-ion momentum spectra with the ADK theory using circularly polarized laser fields. In consideration of the initial distribution of the tunneled electron wave packet in the polarization plane, an improved method based upon Ref. [8] was further proposed [9]. It was also shown that at low laser intensity, i.e., below the saturation intensity, the average intensity can be used to describe the intensity-dependent features in the photoelectron momentum distributions.

In the present study, we measure the photoelectron energy distributions and the momentum distributions from single ionization of xenon atoms in a linearly polarized laser pulse with successively changing the laser intensity. Using the relationship of the photoelectron energy shifted with the ponderomotive energy and the laser intensity, we calibrate the laser peak intensity precisely. We further use the quantum trajectory Monte Carlo (QTMC) approach [10] to simulate the photoelectron energy spectra with respect to the laser peak intensity. The contribution of the resonant and nonresonant ionization has been identified by comparing the measurement with the simulation. Interestingly, inspecting the transverse momentum distribution along the laser propagation axis, we find that the quantum interference has a significant effect on the width of the transverse momentum distributions perpendicular to the laser polarization direction beside the Coulomb focusing effect.

II. EXPERIMENTAL DETAILS

In the experiment, we used a linearly polarized laser pulse (800 nm, 25 fs) from a Ti:sapphire laser system with a repetition of 3 kHz and with amplified pulse energy up to 0.8 mJ. We measured the photoelectron energy distributions and the momentum distributions with respect to the laser intensity using a cold target recoil ion momentum spectroscopy (COLTRIMS) spectrometer [11,12], which has a photoelectron

---

[*] yunquan.liu@pku.edu.cn

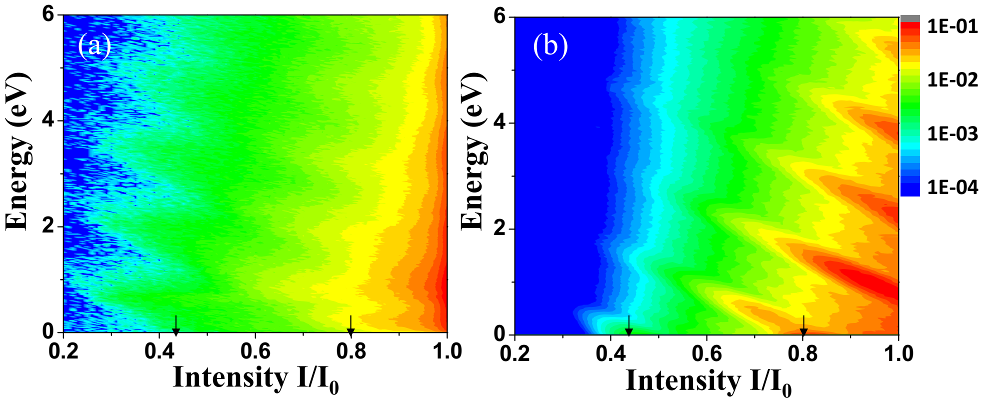

FIG. 1. (Color online) (a) Electron energy spectra of xenon atoms measured in a linearly polarized laser field at 800 nm by successively varying the intensity from $0.2I_0$ to $1.0I_0$, with I_0 the maximum laser peak intensity. (b) Simulation using the QTMC method. The positions of channel closing intensity are indicated by arrows.

momentum resolution ~0.05 a.u. along the transverse direction and ~0.02 a.u. along the time-of-flight direction. Ions and electrons ionized by the laser pulse were accelerated by the spectrometer's homogeneous electric field (~3 V/cm) and magnetic field (~5 G) before hitting the microchannel plate (MCP) detectors along the time-of-flight axis. The positions and the time of flight of the particles were recorded to reconstruct the three-dimensional momentum distributions of the coincident ions and photoelectrons. Experimentally, we successively monitored the laser intensity using a motorized rotary stage to rotate a $\lambda/2$ plate before a thin-film polarizer. The laser polarization direction is along the time-of-flight axis.

III. RESULTS AND DISCUSSIONS

When an atom is exposed to an intensity laser field, the energy levels will shift because of the ac Stark effect. The shift of the ground state can be neglected while the continuum threshold as well as the highly populated excited states will be upshifted by approximately U_p, which is linear dependence on the laser intensity [13]. Figure 1(a) shows the measured photoelectron energy spectra with respect to the laser intensities from single ionization of xenon atoms by a linearly polarized laser pulse. The intensity dependence of the photoelectron energy distributions of the hydrogen atom were theoretically studied [14], whose main features of the electron energy spectra are roughly the same as compared with our experimental measurement. In Fig. 1(a), the horizontal axis represents the relative intensity with respect to I_0, i.e., the maximum peak intensity when successively changing the laser intensity. As the laser intensity increases, the electron wave packet distributions shift towards lower-energy regions due to the increase of the ionization limit. It is conceivable that the photoelectron energy will shift towards zero with further increasing the laser intensity. We refer to this critical laser intensity as the channel closing intensity for the n-photon process (n is the absorbed number of photons), which is indicated by the arrows in Fig. 1(a). Besides, because the ATI order is determined by the number of photons absorbed above the ionization threshold, each order ATI peak can be clearly identified in Fig. 1(a).

In order to reveal the intensity-dependent photoelectron energy spectra clearly, we have normalized the yield [the color scale in Fig. 1(a)] to the maximum value at each laser intensity, as shown in Fig. 2(a). In fact, the expected ATI peaks in the photoelectron energy spectrum should satisfy [2]

$$E_k = n\omega - (I_p + U_p), \tag{1}$$

where I_p is the ionization potential, n is the number of photons absorbed in the process, and ω is the laser frequency. To obtain the relationship between the electron energy and the relative laser intensity, Eq. (1) can be rewritten as

$$E_k = n\omega - I_p - 0.09337 I_0[\mathrm{W/cm^2}]\lambda^2[\mathrm{m}]\frac{I}{I_0}, \tag{2}$$

where λ is the wavelength of the laser pulse, I_0 is the peak laser intensity, and I/I_0 is the relative laser intensity. As predicted, the electron energy of the ATI peak is linear with the laser intensity, as shown by the stripelike structures shown by the dashed lines in Fig. 2(a), According to Eq. (2), the slopes of the line of each order ATI peak with respect to the relative laser intensity is directly related to the peak laser intensity I_0. One can calibrate the peak laser intensity using this slope. We first obtain the slope of the stripelike structure corresponding to each order ATI peak in Fig. 2(a). Taking the average value of the slopes of different n-photon ATI peaks, we can calibrate out the maximum laser intensity $I_0 \sim 7.0 \times 10^{13}\mathrm{W/cm^2}$. We estimate that the uncertainty of the laser intensity calibration, including the systematic errors, is almost 5%. We further calculate the number of photons absorbed in the ATI process, which are indicated by the pure Arabic numbers in Fig. 2(a).

To compare with the experiment results, we have performed the QTMC simulation [10]. Briefly, the laser field is assumed to be polarized in the z direction given by $\vec{F}(t) = F_0 f(t)\sin(\omega t + \varphi_0)\vec{z}$ with $f(t)$ the pulse envelopes, and φ_0 the carrier-envelope phase (CEP), which is set as zero. We use a half-trapezoidal laser pulse with constant pulse envelopes for the first four cycles ramping off within the last three cycles. In the above model, the tunnel exit position along the laser polarization direction is derived from the Landau effective potential theory [15]. At the tunnel exit, the electron wave packet has zero initial longitudinal momentum along the instantaneous laser field and a Gaussianlike transverse momentum distribution perpendicular to the polarization

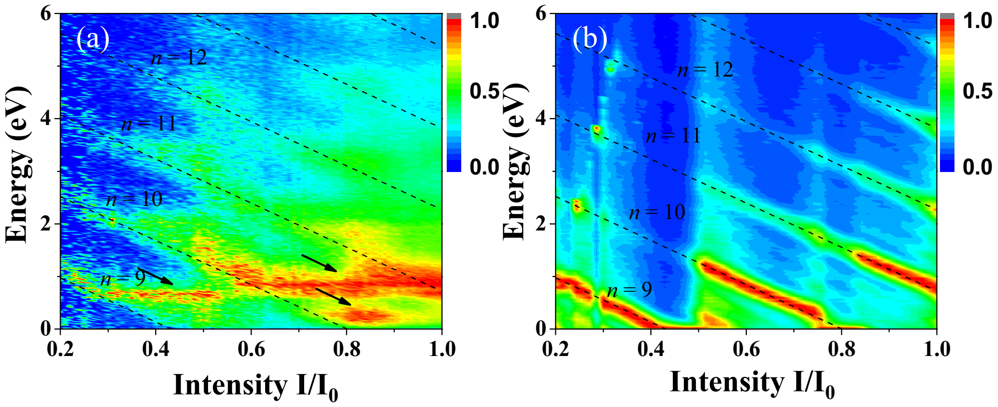

FIG. 2. (Color online) The experimental (a) and the simulated (b) photoelectron energy distributions with respect to the relative laser intensity. The n-photon ATI peaks are denoted by the dashed black lines. The color scale is normalized to the maximum rate for each intensity corresponding to Fig. 1.

direction [16]. The weight of each electron trajectory is given by the ADK ionization rate [17,18] $W(t_0,p_\perp^i) = W_0(t_0)W_1(p_\perp^i)$, where t_0 is the instant of tunneling,

$$W_0(t_0) = [(2I_p)^2/|\vec{F}(t_0)|]^{2/\sqrt{2I_p}-1}\exp[-2(2I_p)^{3/2}/|3\vec{F}(t_0)|], \tag{3}$$

where $W_0(t_0)$ relates to the tunnel phase of the tunneled electrons as well as the ionization potential I_p, and $W_1(p_\perp^i) \propto \sqrt{2I_p}/|\vec{F}(t_0)|\exp[-\sqrt{2I_p}(p_\perp^i)^2/|\vec{F}(t_0)|]$ determines the distributions of the electrons' initial transverse momentum perpendicular to the laser polarization axis. In the three-dimensional semiclassical electron ensemble simulations [19–21], the evolution of the tunneled electrons in the combined Coulomb field and laser field is governed by the Newtonian equation $\ddot{\vec{r}} = -\vec{r}/r^3 - \vec{F}(t)$, with r the distance between the electron and the nucleus. Building on the semiclassical model, the QTMC model encodes the trajectory phase of each tunneled electron with the Feynman path-integral approach and includes the quantum interference effect among the trajectories. The phase of the jth trajectory is expressed as $\phi_j = \int_{t_0}^{\infty}\{\boldsymbol{v}^2(t)/2 - 1/|\boldsymbol{r}(t)| + I_p\}dt$. Since all electrons tunnel from the ground state in the QTMC model, there is no resonant ionization effect. As seen in Fig. 1(b), the simulated photoelectron energy spectrum using the QTMC method agrees well with the measurement except for the resonant structures. In the simulation, the peak intensity is chosen to be in accord with the experimental results with the value of 7.0×10^{13} W/cm^2.

In Fig. 2(b) we show the normalized photoelectron energy spectra versus the relative laser intensity by the QTMC method. The slope of each order ATI peak at different laser intensities in Fig. 2(b) is the same as in Fig. 2(a). Comparing the simulation with the measurement, we find that the main features of the simulated intensity-dependent photoelectron energy spectra are in good agreement with the experimental data. This also indicates that the intensity calibration method using the relationship from the photoelectron energy spectra with respect to the laser intensity is not only intuitive, but also is very precise. According to Eq. (2), the nine-photon and ten-photon channel closing intensities at 800 nm are expected at $\sim 3.0 \times 10^{13}$ W/cm^2 and $\sim 5.6 \times 10^{13}$ W/cm^2, which are in accordance with the experimental observations in Fig. 2(a), as well as in Fig. 2(b).

In the measurement, one can find that some structures in the low-energy region are independent of the laser intensity

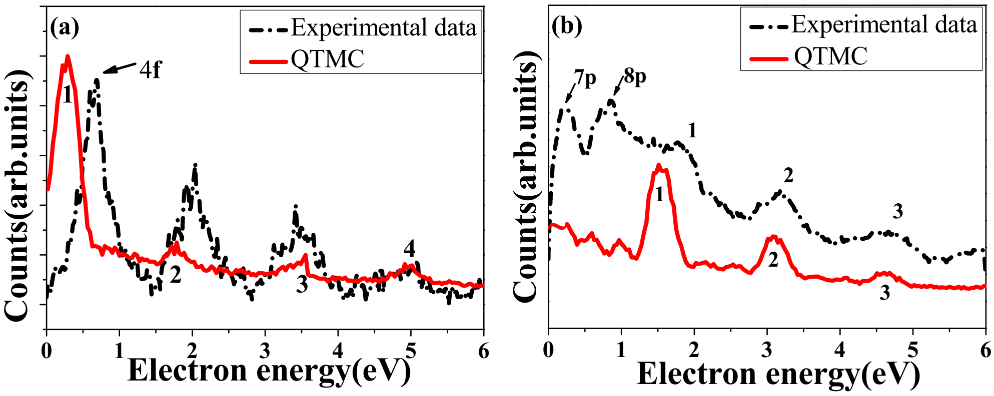

FIG. 3. (Color online) The experimental (black dot-dashed line) and the QTMC simulated (red solid line) photoelectron energy spectra at the intensity of (a) 2.5×10^{13} W/cm^2 and (b) 5.7×10^{13} W/cm^2, respectively. The pure Arabic numbers indicate the ATI order and $4f$, $7p$, and $8p$ indicate the resonant Rydberg states.

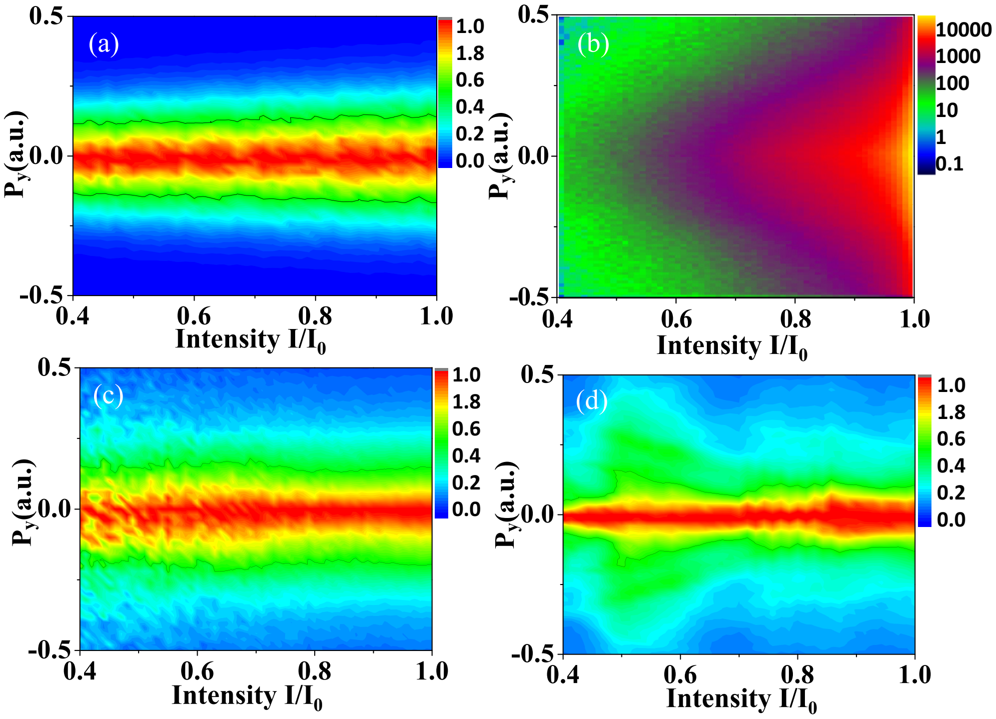

FIG. 4. (Color online) (a) The simulated photoelectron transverse momentum distributions of xenon atoms with respect to laser intensity using the CTMC method. (b) The experimental photoelectron momentum distributions. (c) The same as (b) but normalized to the maximum rate at each laser intensity. (d) The simulated transverse momentum distributions using the QTMC model. The solid lines in (a), (c), and (d) show the position of half maximum of p_y. Note that the color scale is logarithmic in (b).

between two channel closing intensities, which is closely related to the resonantly enhanced ionization via intermediate Rydberg states in the multiphoton regime. These structures can hardly be seen in the QTMC simulation. To see these structures more clearly, we directly compare the measurement with the simulation at specific intensity in Fig. 3.

In Fig. 3(a), we show the measured and the simulated photoelectron energy spectra at the intensity of $I \approx 0.35 I_0 = 2.5 \times 10^{13}$ W/cm^2, which is below the intensity of nine-photon channel closing. Clearly, the main ATI peaks above 1 eV marked by the pure Arabic numbers in the simulation are quantitatively consistent with the measurement. Comparing the simulation with the experiment, one can find that the resonant structure which is absent in the QTMC simulation dominates the ATI spectrum in the low-energy region. We also show the spectra in Fig. 3(b) at the intensity of $I \approx 0.815 I_0 = 5.7 \times 10^{13}$ W/cm^2, which is above the intensity of ten-photon channel closing. One should note here that in the QTMC model all electrons are tunneled from the ground state and there is no resonant ionization effect. So one can isolate the resonant ionization from the ATI process by comparison between the experiment and the simulation. Due to the dipolar parity selection rules, the parity of the resonant Rydberg states at these two laser intensities should be the same [22]. Successive increase of the laser intensity allows identification of the high-lying Rydberg states that manifest themselves as intensity-independent peaks in the electron energy spectrum [23,24]. As shown in Fig. 3(a), in $(8+1)$-photon-ionization channel, the resonant ionization could take place via the $4f$ Rydberg states. In Fig. 3(b), the $(10+1)$-photon resonant ionization will take place via the $7p$ and $8p$ Rydberg states [25]. The comparison between the QTMC simulation and the measurement straightforwardly disentangle the contributions of the resonant ionization and the nonresonant ionization in above-threshold ionization.

Having identified the contribution of the resonant ionization, we have further inspected its effect on the transverse momentum along the laser propagation direction. Generally, the Coulomb focusing effect will narrow the momentum distribution along this direction [26]. As the laser intensity increases, some tunneling electrons are driven back to the ion with higher energy and overpass the ion more quickly. Thus, the narrowing of the transverse momentum distribution caused by the Coulomb focusing will become weaker [27]. Such subjective deduction can be verified by the classical trajectory Monte Carlo (CTMC) simulation [19–21], in which there is no interference effect included. As seen in Fig. 4(a), the width of the simulated transverse momentum distribution increases with the laser intensity. In Fig. 4(b) we illustrate the measured transverse momentum distributions along the laser propagation axis with respect to the laser intensity. To obtain the width of the momentum distribution, we further normalize the yield to the maximum rate at each relative laser intensity, as shown in Fig. 4(c). One can find that the width of the transverse momentum distribution does not increase with the laser intensity, which is in contrast with the simulated result in Fig. 4(a) when removing the interference effect. In Fig. 4(d), we have simulated the transverse momentum distributions along the laser propagation axis using the QTMC method. One can find that the simulated transverse momentum distribution width decreases with respect to the laser intensity in the vicinity of the channel closing intensity, which is consistent with the measurement in Fig. 4(c). It is indicated that the constructive and destructive interference effects of the tunneled electron wave packets will change the width of the momentum distributions transverse to the laser polarization direction.

IV. CONCLUSION

In conclusion, we have measured the intensity-dependent photoelectron energy and momentum spectra of atoms in strong linearly polarized laser fields. The spectra show that, as the laser intensity increases, the ponderomotive shift of above-threshold ionization peaks shifts into the low-energy region because the effective ionization potential is upshifted by the field ponderomotive energy. Using the relationship between the photoelectron energy and the laser intensity, we have calibrated the peak laser intensity precisely. This is an intuitive and accurate method to calibrate the laser peak intensity. We also disentangle the nonresonant and the resonant structures by comparing the measurement with the simulation. We can identify intensity-independent resonant structures from photoelectron energy spectra in the low-energy region. We have also studied the intensity dependence of the final transverse momentum distributions along the laser propagation direction and have shown the importance of the interference effect on the transverse momentum distributions.

ACKNOWLEDGMENTS

This work is supported by the National Program on Key Basic Research Project (Grant No. 2013CB922403), the Natural Science Foundation of China (Grants No. 11434002, No. 11121091, and No. 11134001). Y.L. acknowledges the support by the National Science Fund for Distinguished Young Scholars in China (Grant No. 11125416).

---

[1] P. Agostini, F. Fabre, G. Mainfray, G. Petite, and N. K. Rahman, Phys. Rev. Lett. **42**, 1127 (1979).

[2] G. G. Paulus, F. Grasbon, H. Walther, R. Kopold, and W. Becker, Phys. Rev. A **64**, 021401(R) (2001).

[3] R. R. Freeman, P. H. Bucksbaum, H. Milchberg, S. Darack, D. Schumacher, and M. E. Geusic, Phys. Rev. Lett. **59**, 1092 (1987).

[4] X. Xie, Phys. Rev. Lett. **114**, 173003 (2015).

[5] R. Wiehle, B. Witzel, H. Helm, and E. Cormier, Phys. Rev. A **67**, 063405 (2003).

[6] A. Rudenko, K. Zrost, C. D. Schröter, V. L. B. d. Jesus, B. Feuerstein, R. Moshammer, and J. Ullrich, J. Phys. B **37**, L407 (2004).

[7] V. L. B. d. Jesus, B. Feuerstein, K. Zrost, D. Fischer, A. Rudenko, F. Afaneh, C. D. Schröter, R. Moshammer, and J. Ullrich, J. Phys. B **37**, L161 (2004).

[8] A. S. Alnaser, X. M. Tong, T. Osipov, S. Voss, C. M. Maharjan, B. Shan, Z. Chang, and C. L. Cocke, Phys. Rev. A **70**, 023413 (2004).

[9] C. Smeenk, J. Z. Salvail, L. Arissian, P. B. Corkum, C. T. Hebeisen, and A. Staudte, Opt. Express **19**, 9336 (2011).

[10] M. Li, J. W. Geng, H. Liu, Y. Deng, C. Wu, L. Y. Peng, Q. Gong, and Y. Liu, Phys. Rev. Lett. **112**, 113002 (2014).

[11] R. Dörner, V. Mergel, O. Jagutzki, L. Spielberger, J. Ullrich, R. Moshammer, and H. Schmidt-Böcking, Phys. Rep. **330**, 95 (2000).

[12] J. Ullrich, R. Moshammer, A. Dorn, R. Dörner, L. P. H. Schmidt, and H. Schmidt-Böcking, Rep. Prog. Phys. **66**, 1463 (2003).

[13] R. R. Freeman and P. H. Bucksbaum, J. Phys. B **24**, 325 (1991).

[14] Q. Li, X. M. Tong, T. Morishita, H. Wei, and C. D. Lin, Phys. Rev. A **89**, 023421 (2014).

[15] L. D. Landau and E. M. Lifshitz, *Quantum Mechanics* (Pergamon, New York, 1977).

[16] J. Yuan, M. Li, X. Sun, Q. Gong, and Y. Liu, J. Phys. B **47**, 015003 (2014).

[17] M. V. Ammosov, N. B. Delone, and V. P. Kraĭnov, Zh.Eksp. Teor. Fiz. **91**, 2008 (1986) [Sov. Phys. JETP **64**, 1191 (1986)].

[18] N. B. Delone and V. P. Krainov, J. Opt. Soc. Am. B **8**, 1207 (1991).

[19] B. Hu, J. Liu, and S.G. Chen, Phys. Lett. A **236**, 533 (1997).

[20] H. Liu, Y. Liu, L. Fu, G. Xin, D. Ye, J. Liu, X. T. He, Y. Yang, X. Liu, Y. Deng, C. Wu, and Q. Gong, Phys. Rev. Lett. **109**, 093001 (2012).

[21] M. Li, Y. Liu, H. Liu, Q. Ning, L. Fu, J. Liu, Y. Deng, C. Wu, L. Y. Peng, and Q. Gong, Phys. Rev. Lett. **111**, 023006 (2013).

[22] M. Li, Y. Liu, H. Liu, Y. Yang, J. Yuan, X. Liu, Y. Deng, C. Wu, and Q. Gong, Phys. Rev. A **85**, 013414 (2012).

[23] T. Marchenko, H. G. Muller, K. J. Schafer, and M. J. J. Vrakking, J. Phys. B **43**, 095601 (2010).

[24] T. Marchenko, H. G. Muller, K. J. Schafer, and M. J. J. Vrakking, J. Phys. B **43**, 185001 (2010).

[25] Available at http://physics.nist.gov/cgi-bin/ASD/energy1.pl.

[26] T. Brabec, M. Y. Ivanov, and P. B. Corkum, Phys. Rev. A **54**, R2551(R) (1996).

[27] D. Comtois, D. Zeidler, H. Pepin, J. C. Kieffer, D. M. Villeneuve, and P. B. Corkum, J. Phys. B **38**, 1923 (2005).